

3D Printed High-Throughput Hydrothermal Reactionware for Discovery, Optimization, and Scale-Up**

Philip J. Kitson, Ross J. Marshall, Deliang Long, Ross S. Forgan,* and Leroy Cronin*

Abstract: 3D printing techniques allow the laboratory-scale design and production of reactionware tailored to specific experimental requirements. To increase the range and versatility of reactionware devices, sealed, monolithic reactors suitable for use in hydrothermal synthesis have been digitally designed and realized. The fabrication process allows the introduction of reaction mixtures directly into the reactors during the production, and also enables the manufacture of devices of varying scales and geometries unavailable in traditional equipment. The utility of these devices is shown by the use of 3D printed, high-throughput array reactors to discover two new coordination polymers, optimize the synthesis of one of these, and scale-up its synthesis using larger reactors produced on the same 3D printer. Reactors were also used to produce phase-pure samples of coordination polymers MIL-96 and HKUST-1, in yields comparable to synthesis in traditional apparatus.

3D printing is a technology which has been used in engineering industries to rapidly prototype components for testing prior to traditional manufacturing.^[1] The wide availability of affordable 3D printing facilities is enabled by engineering advances and the decrease in cost of 3D printing equipment, and this has only comparatively recently opened up new opportunities for the use of such techniques beyond established industrial settings. As such, 3D printing approaches are increasingly being used by the scientific community, allowing studies in areas as divergent as the production of tissue-growth scaffolds,^[2] production of biomimetic microvascular systems,^[3] and the manufacture of highly specialized electronic^[4] and pneumatic devices,^[5] as well as the creation of functional devices in laboratory settings.^[6]

Recent work by our group has pioneered the use of 3D printing techniques to produce reactionware in which the outcome of reactions or sequences of reactions can be controlled by the geometry and orientation of the reactionware.^[7] This approach has allowed the fabrication of bespoke

chemical reactors which can be tuned by the individual researcher according to the requirements of individual experiments, however one concern has been the wide chemical, solvent, and temperature compatibility of 3D printed reactionware.^[8] For instance, we wondered if solvothermal synthesis, that is, synthesis in sealed reaction vessels at temperatures above the standard conditions boiling point of the solvent medium, could be possible in 3D printed reactionware. Indeed, hydro- and solvothermal processing is an important technique for the synthesis of a wide range of classes of inorganic materials,^[9] including the production of functional ceramics,^[10] inorganic oxide,^[11] nitride^[12] and chalcogenide^[13] materials, as well as for the synthesis of zeolites^[14] and other nanostructured materials.^[15] Another major use for this technique is the production of novel inorganic cluster materials^[16] and coordination polymers,^[17] but one major drawback of this approach is the expense of the metal hardware (€700 for a 50 mL autoclave), and the limited number of autoclaves usually available to explore a given synthetic parameter space. Added to this, traditionally machined sealed reactors have fixed volumes where it is not easy to perform many small scale test reactions and subsequently scale up the synthesis to prepare larger batch quantities.

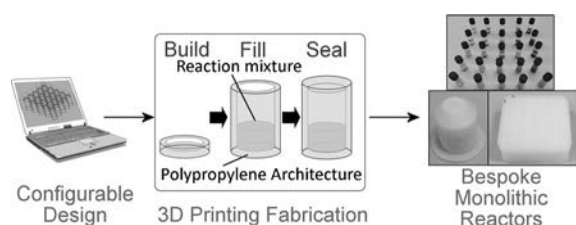
Herein we describe the application of 3D printing techniques to the fabrication of bespoke sealed monolithic reactors which allow the production of adaptable, scalable apparatus ideal for discovery and preparative scale syntheses. Additionally, these techniques allow the facile production of high-throughput devices, where arrays of reaction cavities can be produced simultaneously in one multiplex system, for the scanning of synthetic parameter space. The utility of these high-throughput devices has been demonstrated in their use to rapidly scan a system of ligands to prepare new cadmium- and copper-based three-dimensional coordination polymers. The same 3D printed equipment was then used to investigate the influence of reactant stoichiometries to optimize the synthesis of one of these new materials, and to produce larger reactors for the scale-up of these reactions to preparative quantities.

The unique way in which 3D printing allows objects to be fabricated, in a layer-by-layer fashion building from the bottom of the architecture up, facilitates a new way of introducing material into sealed reactors. Conventional hydrothermal apparatus used in synthetic chemistry consist of a PTFE vessel and lid, which are placed in a machined stainless steel container with a screw-on cap to seal the lid to the body of the PTFE reaction chamber. In contrast, with a 3D printing approach, sealed reactors can be created as single monolithic structures, where the reactant mixtures are

[*] Dr. P. J. Kitson, R. J. Marshall, Dr. D. Long, Dr. R. S. Forgan, Prof. L. Cronin
WestCHEM, School of Chemistry, University of Glasgow
Glasgow G12 8QQ, Scotland (UK)
E-mail: ross.forgan@glasgow.ac.uk
lee.cronin@glasgow.ac.uk
Homepage: <http://www.croninlab.com>

[**] We thank the EPSRC, WestCHEM, and the University of Glasgow for supporting this work. R.S.F. thanks the Royal Society for a URF.

Supporting information for this article is available on the WWW under <http://dx.doi.org/10.1002/anie.201402654>.



Scheme 1. The laboratory manufacturing process of 3D printed sealed reactors for hydrothermal synthesis.

introduced during the fabrication of the structure and so no lid is necessary to seal the reactor volume (see Scheme 1) thus negating the need for expensive precision-machined steel casings to maintain the seals at high pressures. Whilst an initial outlay on 3D printing equipment is required, the nature of 3D printing means that an unlimited number of identical reactors can then be produced for the cost of the materials used (under 20€/Kg in the case of polypropylene, with individual reactors using around 10–20 g of material), making it an economical alternative to traditional apparatus.

Another major advantage of using 3D printing techniques to produce such devices is the ability to reconfigure designs and create bespoke reactors easily, cheaply, and quickly based on designs which are tailored to exact experimental requirements. Thus we were able to produce reactors of varying scales and geometries, including reactors containing spherical voids (see Supporting Information, Section 2) which do not exist as traditional apparatus. As the retrieval of material at the end of the experiment requires the destruction of the seal, this method produces devices which are essentially single-use reactors, reducing the possibility of contamination due to insufficient cleaning between reactions in traditional apparatus, and as the reactors are constructed out of cheap materials this does not add significantly to the overall cost of this method.

All new reactors, **R1–R4**, used in this work were fabricated from polypropylene (PP) using a 3DTouch 3D printer by a fused layer deposition method of 3D printing, whereby successive layers of molten polymer material are laid down in predefined patterns to build up three dimensional structures. Each device was designed using the AutoCAD 2014 3D CAD software package and the printer instruction files were compiled using Axon2 software specific to the 3DTouch system. All the reactors were designed with hollow chambers in the interior of each device surrounded by polypropylene walls of 4 mm thickness. The reactor fabrication process was automatically paused after the print was 80% complete (i.e. before the sealing of the monolith) to allow the introduction of the appropriate reaction mixtures for the desired reaction system. The printing of the device was then restarted and the reactor fabrication completed, yielding a hermetically sealed, monolithic structure which contains the reaction mixture in the void within. The completed device can then be transferred into an oven and heated to the desired temperature to achieve the hydrothermal reaction conditions required. PP was used in the fabrication of these reactors as it produces robust and relatively chemically inert structures, however, the use of thermopolymers to construct high-

temperature devices carries an inherent upper limit to the operating temperatures of the devices. In the case of PP, softening of the polymer begins to occur at approximately 150°C meaning that the structures cannot hold the required pressures for significant lengths of time above this temperature. The nature of high-temperature failure of the 3D printed reactors was observed to be unvarying, occurring at the pre-designed weakest part of the reactor and involved the deformation of the polymer architecture as the plastic softens, causing the device to burst (see Supporting Information, Section 3). However, the design and material of the reactors proved to be sufficient to contain pressures arising from aqueous and aqueous/DMF systems up to 140°C for periods of upwards of 72 h. In all experiments conducted, appropriate secondary containment was used within the heating oven. Full details of safety precautions taken and operating limits used can be found in the Supporting Information.

Proof-of-concept experiments involved the synthesis of known metal–organic frameworks (MOFs) by literature methods. Firstly, the aluminum trimesate based MOF, MIL-96,^[18] was prepared by heating an equimolar solution of Al(NO₃)₃ and trimesic acid dissolved in 1:1 H₂O:DMF (Figure 1). A small-scale PP reactor, with 2 cm diameter

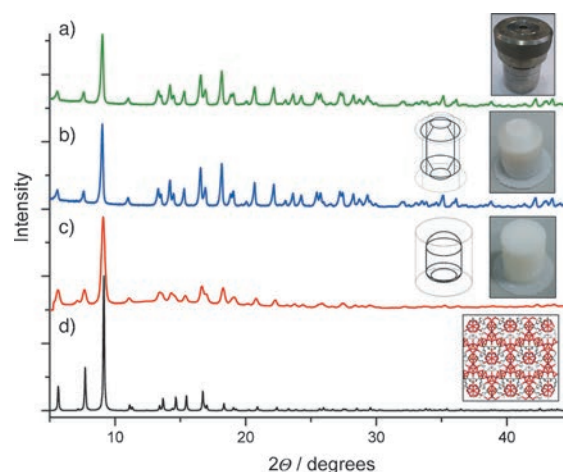


Figure 1. Powder X-ray diffraction patterns of samples of MIL-96 obtained from; a) conventional hydrothermal apparatus (acid digestion vessel, model 4749) manufactured by Parr Instrument Company; b) 20 mL capacity reactor produced by 3D printer (**R2**); c) 3 mL capacity reactor produced by 3D printer (**R1**); d) the calculated pattern from the crystal structure of MIL-96.^[18]

and 3 mL capacity (**R1**), was charged with 2 mL of the reaction mixture during the printing process, and the completed device placed in an oven at 130°C for 18 h. Once the reactor had been allowed to cool slowly to room temperature a drill was used to create a hole in the top of the hydrothermal reactor through which the contents could be extracted. After work up, the white microcrystalline powder exhibited a powder X-ray diffraction pattern very similar to that calculated from the expected crystal structure. Likewise, a larger, 20 mL capacity PP reactor (**R2**) modelled on a conventional Parr reactor, sealed with 10 mL of reactant

solution and heated at 140 °C for 18 h, yielded a white powder, which PXRD analysis showed to be almost identical to the product from a 23 mL Parr acid digestion vessel (model 4749) and both corresponded to the calculated MIL-96 pattern. Yields in both the 3D printed and conventional device were comparable; 60% from the 3D printed reactor compared with 65% from the traditional apparatus. Similarly, the synthesis of HKUST-1,^[19] a copper trimesate prepared in a 1:1 ethanol:water mixture at 120 °C, was facile, with excellent yield and purity (see Supporting information, Section 4), showing the scope of solvents which can be used in the 3D printed PP devices.

Once the principle of using 3D printed devices to effect solvo/hydrothermal syntheses had been established, a new reactor design was developed (**R3**), which consists of a 5 × 5 array of 1 mL capacity reaction chambers, producing a device suitable for high throughput screening of 25 simultaneous, discovery-scale reactions per device. The automated nature of the fabrication allows minimal user interaction during set-up, as most of the printing can occur unattended, for example, overnight, meaning one 5 × 5 reactor (25 reactions) per day per printer is achievable from user contact of less than 1 h. High-throughput hydrothermal apparatus is not unknown,^[20] however these items remain specialized pieces of equipment which are constructed from several pieces of machined PTFE and require similar sealing equipment to those described for traditional hydrothermal equipment. Our 3D printed reactor arrays (Figure 2) were used to investigate the synthetic parameter space of a number of typical diacid (**L1–L5**) linkers and bis(pyridine) based pillars (**P1–P5**) with different metal cations.

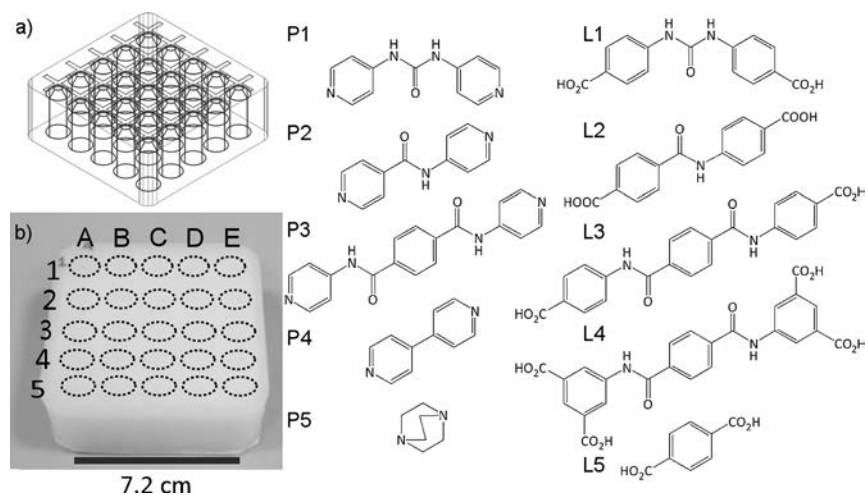


Figure 2. Left: a) Representation of the 3D CAD model of printed reactor **R3**. b) Photograph of the completed reactor depicting the placement of ligands into rows and columns. Center: pyridyl based ligands (**P1–P5**). Right: carboxylic acid based ligands (**L1–L5**).

In a typical high-throughput reaction array (see Supporting Information, Section 5), 0.022 mmol of each diacid ligand were measured into the different rows (1–5) of the device, whilst an equimolar amount of each pillar was measured into the columns (A–E) of the array. Into each well was then

added 0.5 mL of an aqueous 0.05 M $M(\text{NO}_3)_2$ solution followed by 0.1 mL of 0.3 M NaOH solution. Fabrication of the reactor structure was then completed, and the sealed device was briefly sonicated to ensure mixing before being transferred to an oven, where the array was programmably heated to 120 °C for 48 h. After cooling, the reactor was removed from the oven and the individual chambers were opened by drilling holes into the reactor roof and examined for “hits”—samples which yielded single crystals suitable for structure determination—while powders were disregarded. When $\text{Cu}(\text{NO}_3)_2$ was used as the metal-ion source, the majority of the reaction chambers yielded precipitates, however the chamber corresponding to diacid **L5** (terephthalic acid) and pillar **P3** contained, along with some precipitate, purple block crystals suitable for single-crystal X-ray diffraction experiments.

Analysis by X-ray diffraction showed the purple crystals were of $[\text{Cu}(\text{L5-2H})(\text{P3})]_n$, a triply interpenetrated, three-dimensional coordination polymer connected by square-planar four-coordinate copper(II) centers (Figure 3a and b). Ribbons of the bis(pyridyl) pillar **P3** form in one dimension through *trans* coordination to the Cu^{II} ions. Terephthalate dianions extend the structure by forming chains which alternate perpendicularly along the two remaining dimensions, with similar *trans* coordination to the Cu^{II} cations involving only one oxygen atom of the carboxylate groups. The three-fold interpenetration leaves a dense structure with few voids or pores. Many intermolecular short contacts are evident, including a strong hydrogen bond between the amide NH group and free carboxylate OH unit of the adjacent net ($\text{NH}\cdots\text{O}$ 2.86 Å), as well as π - π stacking (3.43 Å) between pyridyl units of the three interpenetrated nets.

Repeating the discovery experiment with $\text{Cd}(\text{NO}_3)_2$ as the metal source generated further hits. Again, the chamber containing ligand terephthalic acid (**L5**), the bis(amido) pillar **P3** and the Cd^{2+} source yielded crystalline material, which was analyzed by single-crystal diffraction. $[\text{Cd}(\text{L5-2H})(\text{P3})]_n$ has a similar empirical formula to the previous coordination polymer but a completely different network structure (Figure 3c,d). The material has a twofold interpenetrated structure composed of cadmium terephthalate sheets linked into three dimensions by molecules of **P3**. A dimeric Cd^{II} structural building unit (SBU) is present, wherein single Cd^{2+} ions are coordinated by two bridging terephthalate dianions—providing one oxygen donor to each metal center—and one dianion each which coordinates to each Cd center through both its oxygen atoms. The remaining two axial coordination sites on each cation are occupied by pyridine nitrogen atoms from pillar units, with π - π stacking interactions (3.44 Å) occurring between these adjacent aromatic rings. Despite the relatively

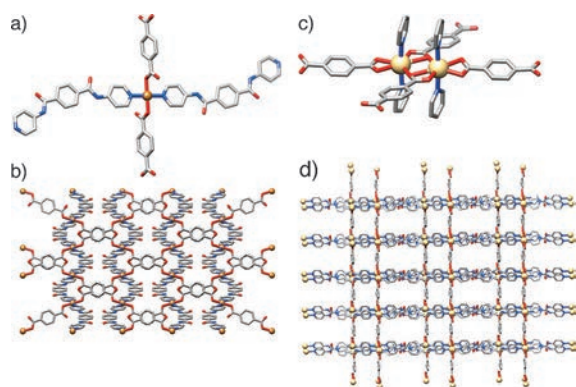


Figure 3. The solid-state structures of the two coordination polymers discovered in the 3D printed reactor arrays. a) Primary coordination environment of Cu^{II} in $[\text{Cu}(\text{L5-2H})(\text{P3})]_n$. b) Ball and stick representation of the packing of $[\text{Cu}(\text{L5-2H})(\text{P3})]_n$. c) Primary coordination environment of the dimeric Cd^{II} subunit in $[\text{Cd}(\text{L5-2H})(\text{P3})]_n$. d) Ball and stick representation of the packing of $[\text{Cd}(\text{L5-2H})(\text{P3})]_n$. Cu orange, Cd yellow, N blue, O red, C gray.

dense interpenetrated packing structure, one-dimensional voids filled with waters of crystallization are apparent, which, upon removal of these interstitial solvents, may endow the network with permanent porosity. Along with this second coordination polymer, crystals of the known discrete complexes $[\text{Cd}(\text{4-aminobenzoate})_2(\text{H}_2\text{O})] \cdot 2\text{H}_2\text{O}$ (CCDC ABZCUH02)^[21] and $[\text{Cd}(\text{isonicotinate})_2(\text{H}_2\text{O})_4]$ (CCDC code INICCD02)^[22] were isolated from the hydrothermal decomposition of **L1** and **P2**, respectively, under the reaction conditions.

As the initial synthesis of $[\text{Cu}(\text{L5-2H})(\text{P3})]_n$ also yielded a light blue precipitate alongside the purple crystalline material, the 3D printed reactor arrays were used to investigate further the synthetic parameter space to optimize the synthesis of the coordination polymer (see Supporting Information, Section 6). 5×5 high throughput arrays of hydrothermal experiments were performed which systematically varied the synthetic conditions in the $[\text{Cu}(\text{L5-2H})(\text{P3})]_n$ system. This multi-parameter variation allows the construction of a 2D map of reaction conditions (Figure 4) from each array experiment to pinpoint the reaction conditions necessary to achieve optimum phase-purity prior to scaling-up to preparative quantities. Equimolar mixtures of **P3** and **L5**, as determined by the stoichiometry from the crystal structure, were treated with solutions containing different concentrations of $\text{Cu}(\text{NO}_3)_2$ and NaOH and subjected to the same hydrothermal conditions as described above. The samples from each of the individual reaction wells were collected, dried and homogenized before being characterized by powder X-ray diffraction (PXRD), from which the different compositions of the individual wells can be identified. Six distinct species could be observed in the reaction products with most reaction chambers containing some combination of two or more of the species. High $[\text{OH}^-]:[\text{Cu}]$ ratios were characterized by CuO precipitate, along with unreacted **P3**. Conversely, low $[\text{OH}^-]:[\text{Cu}]$ ratios tended to produce green/blue precipitates of $[\text{Cu}_2(\text{L5-2H})(\text{OH})_2]_n$ ^[23] with the intervening conditions producing varying proportions of these species. Two

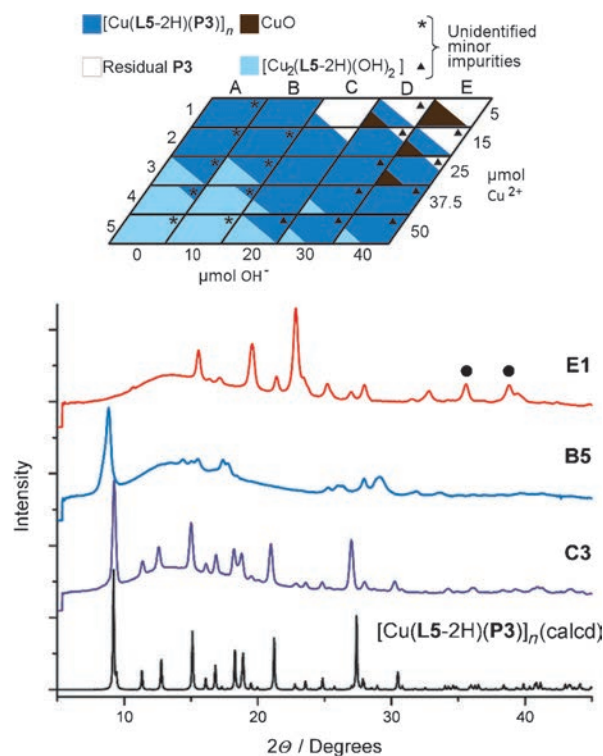


Figure 4. Top: 2D map illustrating the reaction products arising from the $\text{Cu}(\text{NO}_3)_2/\text{P3}/\text{L5}/\text{NaOH}$ system. Bottom: Powder X-ray diffraction patterns arising from the contents of reaction wells E1, B5, and C3, and the expected pattern for $[\text{Cu}(\text{L5-2H})(\text{P3})]_n$ as calculated from its single-crystal structure. Peaks arising from CuO are indicated by black circles.

minor but distinct impurities were also observed amongst the reaction products, one of which occurred generally at low NaOH concentrations and the other at high NaOH concentrations. These impurities were never present in sufficient quantities to allow identification, but it is possible that they arise from the partial decomposition of **P3**. Each well also contained a small proportion of amorphous material, as indicated by some broad features in the PXRD patterns. However this material was not present in sufficient quantities to prevent scale-up and isolation of $[\text{Cu}(\text{L5-2H})(\text{P3})]_n$ in good yields (see below).

Analysis of the composition of the products allowed the identification of conditions which could be scaled up to a preparative scale using the 20 mL capacity reactor **R2**. After heating the reactor to 120°C for 48 h, the resulting purple crystalline $[\text{Cu}(\text{L5-2H})(\text{P3})]_n$ was washed with water and methanol, yielding a pure sample of $[\text{Cu}(\text{L5-2H})(\text{P3})]_n$. The same procedure was followed using the same quantities of material in commercial 23 mL Parr hydrothermal-synthesis equipment. The purity of the products from both the traditional and 3D printed apparatus were compared by powder X-ray diffraction and found to be comparable (see Supporting Information, Section 7), with the only appreciable difference being a slight reduction in individual crystal size from the 3D printed reactor.

In conclusion, 3D printing techniques have been used to fabricate disposable monolithic hydrothermal reactors from

polypropylene which are suitable for conducting reactions at elevated temperatures and pressures. The nature of their fabrication means various designs of reactor can be fabricated on a single printer, allowing the production of varying scales of devices from 1 mL discovery reactors to 20 mL capacity reactors suitable for preparative scale reactions. 5×5 arrays of small scale reactors have been fabricated to allow high-throughput hydrothermal investigation of reaction systems. This apparatus has been used to prepare phase pure samples of literature MOFs MIL-96 and HKUST-1, and high-throughput devices were used to investigate several new pyridyl and carboxylic acid derived ligands for inorganic synthesis, resulting in the discovery of two new three dimensional coordination polymers, $[\text{Cu}(\text{L5-2H})(\text{P3})]_n$ and $[\text{Cd}(\text{L5-2H})(\text{P3})]_n$. The 5×5 array reactors were then used to investigate the synthetic conditions used in the synthesis of $[\text{Cu}(\text{L5-2H})(\text{P3})]_n$ allowing the scale up of the synthesis to preparative quantities, with no loss of purity compared to traditional hydrothermal apparatus. The application of 3D printing technologies to reactors such as these demonstrates the unprecedented control and efficiency these techniques can offer experimenters over both the form and function of experimental equipment. Work is continuing to develop the 3D printing of alternative polymers, which will extend the temperature range of utility of these devices whilst retaining the chemical resistance. We are also developing polymers which can take an active role in the progress of reactions and have added nanoparticle catalysts in the polymer walls for example. Additional surface modifications, to take part in the reactions as well as aid crystallization, are also being investigated.

Experimental Section

Caution: Extreme care must be exercised when operating sealed reactors containing solvents at high temperatures. Appropriate safety equipment and secondary containment was used at all times in this study. 3D printing was achieved on a Bits from Bytes (BfB) 3DTouchTM 3 extruder 3D printer supplied by Bits from Bytes, using Polypropylene (PP) supplied by Barnes Plastic Welding Equipment Ltd., Blackburn, UK. For detailed experimental conditions and chemical/crystallographic analysis see the Supporting Information. CCDC 988015 ($[\text{Cu}(\text{L5-2H})(\text{P3})]_n$), 988016 ($[\text{Cd}(\text{L5-2H})(\text{P3})]_n$) contain the supplementary crystallographic data for this paper. These data can be obtained free of charge from The Cambridge Crystallographic Data Centre via www.ccdc.cam.ac.uk/data_request/cif.

Received: February 21, 2014

Revised: June 5, 2014

Published online: July 30, 2014

Keywords: 3D printing · coordination polymers · high-throughput synthesis · hydrothermal synthesis · reactor design

- [1] a) D. Dimitrov, K. Schreve, N. de Beer, *Rapid Prototyping J.* **2006**, *12*, 136–147; b) D. T. Pham, R. S. Gault, *Int. J. Mach. Tool. Manu.* **1998**, *38*, 1257–1287.
- [2] a) J. L. Connell, E. T. Ritschdorff, M. Whiteley, J. B. Shear, *Proc. Natl. Acad. Sci. USA* **2013**, *110*, 18380–18385; b) V. Mironov, T. Boland, T. Trusk, G. Forgacs, R. R. Markwald, *Trends Biotechnol.* **2003**, *21*, 157–161; c) S. M. Peltola, F. P. W. Melchels, D. W. Grijpma, M. Kellomäki, *Ann. Med.* **2008**, *40*, 268–280; d) H. Seitz, W. Rieder, S. Irsen, B. Leukers, C. Tille, *J. Biomed. Mater. Res. Part B* **2005**, *74*, 782–788.
- [3] a) K. Pataky, T. Braschler, A. Negro, P. Renaud, M. P. Lutolf, J. Brugger, *Adv. Mater.* **2012**, *24*, 391–396; b) D. Therriault, S. R. White, J. A. Lewis, *Nat. Mater.* **2003**, *2*, 265–271.
- [4] B. Y. Ahn, E. B. Duoss, M. J. Motala, X. Y. Guo, S. I. Park, Y. J. Xiong, J. Yoon, R. G. Nuzzo, J. A. Rogers, J. A. Lewis, *Science* **2009**, *323*, 1590–1593.
- [5] a) F. Ilievski, A. D. Mazzeo, R. F. Shepherd, X. Chen, G. M. Whitesides, *Angew. Chem.* **2011**, *123*, 1930–1935; *Angew. Chem. Int. Ed.* **2011**, *50*, 1890–1895; b) S. A. Morin, R. F. Shepherd, S. W. Kwok, A. A. Stokes, A. Nemiroski, G. M. Whitesides, *Science* **2012**, *337*, 828–832; c) T. Hasegawa, K. Nakashima, F. Omatsu, K. Ikuta, *Sens. Actuators A* **2008**, *143*, 390–398.
- [6] a) K. B. Anderson, S. Y. Lockwood, R. S. Martin, D. M. Spence, *Anal. Chem.* **2013**, *85*, 5622–5626; b) T. A. Campbell, O. S. Ivanova, *Nano Today* **2013**, *8*, 119–120; c) P. Nikolaou, A. M. Coffey, L. L. Walkup, B. M. Gust, C. D. LaPierre, E. Koehnemann, M. J. Barlow, M. S. Rosen, B. M. Goodson, E. Y. Chekmenev, *J. Am. Chem. Soc.* **2014**, *136*, 1636–1642; d) A. I. Shallan, P. Smejkal, M. Corban, R. M. Guijt, M. C. Breadmore, *Anal. Chem.* **2014**, *86*, 3124–3130.
- [7] M. D. Symes, P. J. Kitson, J. Yan, C. J. Richmond, G. J. T. Cooper, R. W. Bowman, T. Vilbrandt, L. Cronin, *Nat. Chem.* **2012**, *4*, 349–354.
- [8] a) V. Dragone, V. Sans, M. H. Rosnes, P. J. Kitson, L. Cronin, *Beilstein J. Org. Chem.* **2013**, *9*, 951–959; b) P. J. Kitson, M. H. Rosnes, V. Sans, V. Dragone, L. Cronin, *Lab Chip* **2012**, *12*, 3267–3271; c) P. J. Kitson, M. D. Symes, V. Dragone, L. Cronin, *Chem. Sci.* **2013**, *4*, 3099–3103; d) J. S. Mathieson, M. H. Rosnes, V. Sans, P. J. Kitson, L. Cronin, *Beilstein J. Nanotechnol.* **2013**, *4*, 285–291.
- [9] a) G. Demazeau, *J. Mater. Sci.* **2008**, *43*, 2104–2114; b) R. I. Walton, *Chem. Soc. Rev.* **2002**, *31*, 230–238.
- [10] K. J. Zhu, L. K. Su, H. L. Ji, J. H. Qiu, L. Bai, K. Yanagisawa, K. Kajiyoshi, *J. Inorg. Mater.* **2010**, *25*, 1159–1163.
- [11] a) T. R. Amarante, P. Neves, A. A. Valente, F. A. Almeida Paz, A. N. Fitch, M. Pillinger, I. S. Gonçalves, *Inorg. Chem.* **2013**, *52*, 4618–4628; b) M. Kobayashi, K. Tomita, V. Petrykin, M. Yoshimura, M. Kakihana, *J. Mater. Sci.* **2008**, *43*, 2158–2162.
- [12] B. Mazumder, P. Chirico, A. L. Hector, *Inorg. Chem.* **2008**, *47*, 9684–9690.
- [13] X. Jiang, W. Xu, R. Tan, W. Song, J. Chen, *Mater. Lett.* **2013**, *102–103*, 39–42.
- [14] a) C. S. Cundy, P. A. Cox, *Microporous Mesoporous Mater.* **2005**, *82*, 1–78; b) W. C. Yoo, S. Kumar, Z. Wang, N. S. Ergang, W. Fan, G. N. Karanikolos, A. V. McCormick, R. L. Penn, M. Tsapatsis, A. Stein, *Angew. Chem.* **2008**, *120*, 9236–9239; *Angew. Chem. Int. Ed.* **2008**, *47*, 9096–9099.
- [15] a) Y. Fang, D. Gu, Y. Zou, Z. Wu, F. Li, R. Che, Y. Deng, B. Tu, D. Zhao, *Angew. Chem.* **2010**, *122*, 8159–8163; *Angew. Chem. Int. Ed.* **2010**, *49*, 7987–7991; b) K. Tomita, V. Petrykin, M. Kobayashi, M. Shiro, M. Yoshimura, M. Kakihana, *Angew. Chem.* **2006**, *118*, 2438–2441; *Angew. Chem. Int. Ed.* **2006**, *45*, 2378–2381.
- [16] a) D. M. Low, L. F. Jones, A. Bell, E. K. Brechin, T. Mallah, E. Rivière, S. J. Teat, E. J. L. McInnes, *Angew. Chem.* **2003**, *115*, 3911–3914; *Angew. Chem. Int. Ed.* **2003**, *42*, 3781–3784; b) L. M. Rodriguez-Albelo, G. Rousseau, P. Mialane, J. Marrot, C. Mellot-Draznieks, A. R. Ruiz-Salvador, S. Li, R. Liu, G. Zhang, B. Keita, A. Dolbecq, *Dalton Trans.* **2012**, *41*, 9989–9999; c) T. M. Smith, K. Perkins, D. Symester, S. R. Freund, J. Vargas, L. Spinu, J. Zubieta, *CrystEngComm* **2014**, *16*, 191–213.

- [17] a) M. L. Foo, S. Horike, Y. Inubushi, S. Kitagawa, *Angew. Chem.* **2012**, *124*, 6211–6215; *Angew. Chem. Int. Ed.* **2012**, *51*, 6107–6111; b) S. K. Ghosh, S. Bureekaew, S. Kitagawa, *Angew. Chem.* **2008**, *120*, 3451–3454; *Angew. Chem. Int. Ed.* **2008**, *47*, 3403–3406; c) H. Deng, S. Grunder, K. E. Cordova, C. Valente, H. Furukawa, M. Hmadeh, F. Gándara, A. C. Whalley, Z. Liu, S. Asahina, H. Kazumori, M. O’Keeffe, O. Terasaki, J. F. Stoddart, O. M. Yaghi, *Science* **2012**, *336*, 1018–1023; d) N. A. Vermeulen, O. Karagiari, A. A. Sarjeant, C. L. Stern, J. T. Hupp, O. K. Farha, J. F. Stoddart, *J. Am. Chem. Soc.* **2013**, *135*, 14916–14919; e) O. K. Farha, J. T. Hupp, *Acc. Chem. Res.* **2010**, *43*, 1166–1175.
- [18] T. Loiseau, L. Lecroq, C. Volkringer, J. Marrot, G. Férey, M. Haouas, F. Taulelle, S. Bourrelly, P. L. Llewellyn, M. Latroche, *J. Am. Chem. Soc.* **2006**, *128*, 10223–10230.
- [19] S. S. Y. Chui, S. M. F. Lo, J. P. H. Charmant, A. G. Orpen, I. D. Williams, *Science* **1999**, *283*, 1148–1150.
- [20] a) P. M. Forster, N. Stock, A. K. Cheetham, *Angew. Chem.* **2005**, *117*, 7780–7784; *Angew. Chem. Int. Ed.* **2005**, *44*, 7608–7611; b) N. Stock, *Microporous Mesoporous Mater.* **2010**, *129*, 287–295; c) P. Maniam, N. Stock, *Inorg. Chem.* **2011**, *50*, 5085–5097.
- [21] D. A. Clemente, A. Marzotto, *Acta Crystallogr. Sect. B* **2004**, *60*, 287–292.
- [22] L. Shen, J. Liu, Y. Xu, *J. Coord. Chem.* **2002**, *55*, 123–127.
- [23] S. Abdelouhab, M. François, E. Elkaim, P. Rabu, *Solid State Sci.* **2005**, *7*, 227–232.
-